Local Segmental Dynamics of Poly(2-hydroxyethyl Methacrylate) in Methanolic Solution by Spin Label X-Band ESR†

Antonín Marek, Jiří Czernek, Miloš Steinhart, Jiří Labský, Petr Štěpánek, and Jan Pilař*

Institute of Macromolecular Chemistry, Academy of Sciences of the Czech Republic, 162 06 Prague 6, Czech Republic

Received: July 17, 2003; In Final Form: November 5, 2003

A copolymer of 2-hydroxyethyl methacrylate (HEMA) with spin-labeled methacrylic acid units distributed randomly along the main chain (∼3 mol %) was synthesized. ESR spectra of methanolic solutions of the copolymer at concentrations ranging from 2 to 50 wt % were measured at X-band (9 GHz) over a broad temperature range. Temperature dependence of the parameter R_S, characterizing the local segmental dynamics in PHEMA chain, and of the other parameters characterizing local dynamics and conformation of the copolymer were determined by fitting experimental ESR spectra to the theoretical spectra calculated using the MOMD model. Arrhenius plots of the rotational parameters exhibit atypical nonlinear behavior characterized by two breaks at particular temperatures in the R_S plot. It is concluded that, similarly to PMMA in a number of solvents, PHEMA in methanol undergoes a conformational transition from a less compact to more compact conformation of the polymer chain when the temperature increases in a particular temperature range. Results of dynamic light scattering and X-ray scattering experiments support this conclusion. Analysis of the shape of the ordering potential, which constrains the preferred orientation of the effective axis of internal rotation of the tethered nitroxide, revealed the occurrence of two different conformations of the nitroxide moiety. Based on the results of quantum chemical calculations, two conformations of the model system (nitroxide plus tether) are proposed, which are in a good agreement with the geometry required by the ordering potentials.

Introduction

Study of local segmental dynamics of polymers plays a significant role in understanding structure−property relationships shown by different polymers. These relationships are an important subject in polymer research. It is useful to study local chain motions of an isolated chain in dilute solutions before chain−chain interactions are taken into account. Dynamics on the length scale of a few monomer units depends strongly on the conformation of the polymer chain in dilute solution, mainly as a result of polymer−solvent interactions. In recent years a great deal of effort has been devoted to understanding the local dynamics of polymers by measuring the correlation time, τ_c, for segmental rotational diffusion of polymers in dilute solution. Measurement of the fluorescence depolarization of the anthracene chromophore bonded inside the main chain[1−14] and measurement of ^{13}C NMR relaxation times and NOE values[15−23] have been used for this purpose. Computer simulation studies have also been performed.[24−26]

Data characterizing local rotational dynamics of polymer chain in solution can be obtained by ESR of spin-labeled polymers as well.[27−30] Parameters characterizing rotational diffusion of nitroxide spin labels embedded in a particular system may be determined by analysis of their ESR spectra.[31] Rotational diffusion of the nitroxide spin label, which is attached to chain segments of a polymer at randomly distributed sites, has been approximated by superposition of the isotropic rotational diffusion of the polymer chain segment, as characterized by rotational diffusion coefficient, R_S, and by the internal rotation of the spin label about the tether through which it is attached to the polymer chain segment, which is characterized by the rotational diffusion coefficient, R_l.[27−30] The contribution of rotational diffusion of the polymer coil as a whole has been neglected for high-molecular-weight polymers. When the spin label is attached to the polymer chain via a short tether containing only one single bond through which conformational transitions of the tether can occur, then the axis of internal rotation of the spin label should be identical to this bond axis. This approximate model gives rise to axially symmetric rotational diffusion with two components of the rotational tensor, $R_{prp} = R_S$ and $R_{pll} = R_S + R_l$. In addition, the axis of internal rotation can be tilted by angle β relative to the z axis in the xz plane of the nitroxide axis system (regarding the symmetry plane of the piperidine ring). This is shown in Chart 1 for the 2,2,6,6-tetramethylpiperidin-1-yloxyl type spin label. In this case the

CHART 1

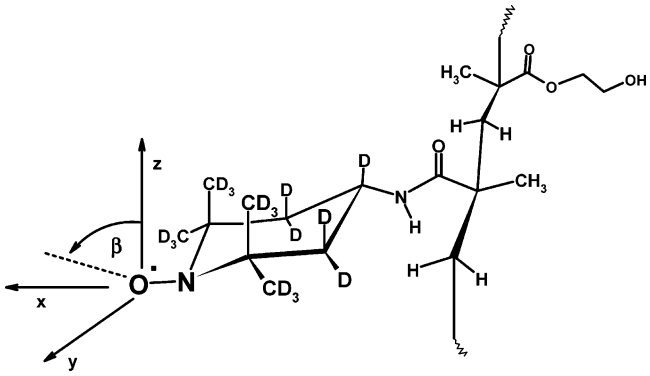

† Part of the special issue "Jack H. Freed Festschrift".

* Corresponding author. E-mail: pilar@imc.cas.cz.

10.1021/jp036083y CCC: $27.50
Published on Web 03/17/2004

tether involves three single bonds (C−CO, CO−NH, and NH−SL, where SL stands for 2,2,6,6-tetramethylpiperidin-1-yloxyl). Given that the second bond, which is a peptide bond, can be considered to be fixed regarding the time window of the relevant motions, and that there are steric constraints around the first bond, the only bond through which conformational changes of the tether are expected to occur is the NH−SL bond.

At the X-band ESR frequency (9 GHz), rotational dynamics in most fluids is usually sufficiently fast, i.e., $\tau_R\Delta\omega \ll 1$ (where the correlation time, $\tau_R = 6^{-1}(R_{prp}{}^2R_{pll})^{-1/3}$, and $\Delta\omega$ is a measure of the magnitude of the orientation-dependent part of the spin Hamiltonian), and such motions fall within the motional narrowing regime. In such cases the ESR spectrum is a simple superposition of Lorentzian lines whose widths cannot be fully and unambiguously related to parameters characterizing the nitroxide rotational diffusion by the motional narrowing theory without additional assumptions on the motion. For slower motions, in more viscous media where $\tau_R\Delta\omega \geq 1$, the ESR spectrum depends more dramatically on the combined influence of molecular motion and magnetic interactions. Thus, the slow-motional ESR line shapes, in principle, provide a more detailed picture of rotational dynamics when compared with motionally narrowed line shapes. These slow-motional line shapes can be fully analyzed using a theoretical approach based on numerical solution of the stochastic Liouville equation.[31,32]

In recent papers[30,33] we have presented results of ESR studies of segmental dynamics of spin labeled polystyrene in dilute solutions in a broad range of solvents. Using spectral analysis based on the stochastic Liouville equation,[31,32] we have shown that the MOMD (microscopic order with macroscopic disorder) model introduced by Meirovitch et al.[31,34] is very successful in analyzing ESR line shapes of spin-labeled polymers. This model allows for constraints in the above-mentioned motions. More precisely, we consider the polymer chain segmental motion sensed by the tethered nitroxide, i.e., the wobbling motion of the effective axis of internal rotation, as constrained by an orienting potential, typically given by

$$-U(\theta,\varphi)/kT = \sum_{L=2,4}\{c_0^L D_{00}^L(\theta,\varphi) + c_2^L[D_{02}^L(\theta,\varphi) + D_{0-2}^L(\theta,\varphi)]\} \quad (1)$$

where the c_0^L terms refer to the strength and shape of the restricting potential for the wobbling motion and the c_2^L to its asymmetry, and D_{0K}^L (θ,φ) are Wigner rotation matrix elements. The angles θ and φ are the polar and azimuthal angle, respectively, characterizing orientation of the effective axis of internal rotation relative to the director expressed in the principal axes of nitroxide rotational diffusion tensor.

Hydrogels are polymer materials which have the ability to retain substantial amounts of water and show soft and rubbery-like consistency.[35] Hydrogels based on the HEMA monomer exhibit excellent biocompatibility and physical properties similar to those of living tissue.[36,37] For these reasons they have found large-scale applications in medical practice.[38] In particular, material based on such hydrogels has been used for manufacturing soft contact and intraocular lenses.[39] We have recently described the translational macroscopic diffusion of various paramagnetic tracers in HEMA-based gels equilibrium-swollen with methanol, and in PHEMA methanolic solutions measured by one-dimensional electron spin resonance imaging (1D ESRI).[40] Insolubility of linear PHEMA in water precludes a comparison of the diffusion in cross-linked HEMA gels and in PHEMA solutions in aqueous media. As the next step in the study of HEMA-based polymer systems, we present here an investigation of local segmental dynamics of spin-labeled PHEMA in methanolic solution over a wide concentration range. To the best of our knowledge, measurements characterizing local polymer dynamics of PHEMA have not been reported so far, and data on local dynamics in nondilute solutions can only scarcely be found in the literature.

Experimental Section

Synthesis and Characterization of Spin Labeled PHEMA. 2-Hydroxyethyl methacrylate (HEMA) (Fluka) **(I)** (8 g) was copolymerized with *N*-(3,3,5,5-tetra[^{2}H]-2,2,6,6-tetra([$^2H_3$]-methyl)piperidin-4-yl)methacrylamide **(II)** (0.45 g) in ethanolic solution (50 mL) using 2,2′-azobis(isobutyronitrile) (ABIN) as an initiator (0.3 g, 65 °C, 7 h), and the copolymer obtained **(III)** was precipitated in ether (500 mL). In the second step, the amino groups in the copolymer **(III)** (10 g) were oxidized in methanolic solution by adding sodium tungstate (0.5 g), EDTA (0.5 g), and 30 mL of 30% hydrogen peroxide and stirring in the dark for 10 days. The spin-labeled PHEMA **(IV)** was precipitated into a 1:1 mixture ether/acetone (500 mL). No unoxidized amine was found in **(IV)** by NMR. *N*-(3,3,5,5-tetra-[^{2}H]-2,2,6,6-tetra([$^2H_3$]methyl)piperidin-4-yl)methacrylamide) was synthesized using the procedure described by Kurosaki et al.[41] from 4-amino-3,3,5,5-tetra[^{2}H]-2,2,6,6-tetra([$^2H_3$]methyl)-piperidine, which was prepared as described earlier.[42] The mass-average molecular weight, M_w, equal to 9.5×10^4, was determined by light scattering measurements in methanol at 633 nm and 25 °C using a modified Sofica 42.000 instrument. Refractive index increments were measured under the same conditions using a Brice-Phoenix BP-2000 V differential refractometer. Concentration of the spin-labeled monomer units, ∼3 mol %, was determined by ESR.

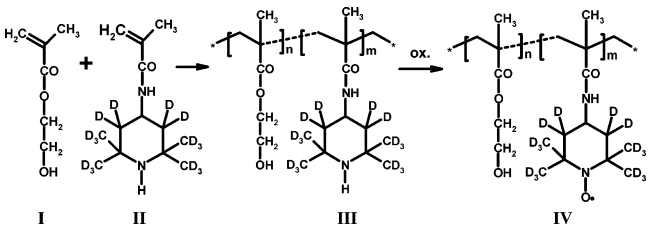

ESR Measurements. X-band ESR spectra were recorded over a suitable temperature range using Bruker ELEXSYS E−540 spectrometer. An amount of spin-labeled PHEMA **(IV)** corresponding to the desired concentration was dissolved in methanol, homogenized for at least 10 days, and filled into quartz capillaries (o.d. approximately 1 mm). The measurements were performed with 100 kHz magnetic field modulation at a microwave output of 2 mW.

Analysis of ESR Spectra. In the first step of the analysis, the ***A***- and ***g***-tensors of the spin label attached to the PHEMA were determined by analyzing rigid-limit spectra of the spin-labeled polymer in methanolic solvent at particular concentration. Theoretical rigid-limit spectra were calculated with the EPRR program[31] and compared with the experimental rigid-limit spectra using an added optimization routine. The EPRR program was extended by including the Pearson VII peak function as another approximation to the line shape. This function is defined in one dimension by an expression

$$f(x) = H\{1 + [2(x - x_0)(2^{1/M} - 1)^{1/2}/w^P]^2\}^M \quad (2)$$

where M is the Pearson parameter which for lines that are

Lorentzian in character approaches unity and for Gaussian lines approaches infinity, w^P is the full width at half-maximum of the line, x_0 is the center of the distribution, and H is normalization constant. ***A***- and ***g***-tensor components, the Pearson parameter M, and components of the axially symmetric tensor of Pearson line widths w^P_{prp} and w^P_{pll} were fitted during the analysis. The presence of the ordering potential was not considered in the case of rigid-limit spectra. The principal axis systems of both tensors were considered identical; their tensor components were assumed to be temperature independent.

Slow-motional ESR spectra were calculated utilizing the spectral simulation method based on the stochastic Liouville equation.[31] The slow-motional simulated spectra were fitted to the experimental spectra using a PC version of the NLSL program[32] based on a modified Levenberg−Marquart minimization algorithm, which iterates the simulations until a minimum least-squares fit to the experiment is reached. This provides optimum values for the fitted parameters together with error estimates. The values of the ***A***- and ***g***-tensor components were fixed throughout the analysis of slow-motional ESR spectra in the particular solvent. The MOMD model[31,34] for spin-label rotational diffusion was assumed. In this case fitted parameters include the parallel and perpendicular rotational diffusion coefficients R_{pll} and R_{prp}, the diffusion tilt, β, the inhomogeneous Lorentzian broadening, w^L, and the parameters c^L_0 and c^L_2 characterizing the ordering potential. When all c^L_0 and c^L_2 are zero, one obtains simple Brownian rotational diffusion. All spectral simulations were performed on a 2 GHz PC.

Dynamic Light Scattering (DLS). Dynamic light scattering measurements have been performed using a home-built goniometer, a 35 mW Helium−Neon laser Spectra-Physics 125A, and an ALV5000/E correlator operated in the cross-correlation mode. Light scattered by the sample was collected at an angle of 90° by an optical fiber including a beam-splitter, the fiber outputs of which were connected to two avalanche photodiode decetectors. The signals of these detectors were cross-correlated to eliminate the influence of after-pulsing on the correlation curve. The temperature was regulated in the range −60 °C to 60 °C by a Lakeshore 330 controller working against a cold source of vapors of liquid nitrogen flowing through the sample holder. From the measured intensity correlation function $g_2(t)$, the distribution $A(\tau)$ of relaxation times τ was calculated by performing the inverse Laplace transformation $g_2(t) = [1 + \beta \int A(\tau)\ \exp(-t/\tau)\ d\tau]^2$ using the program REPES.[43] The hydrodynamic radius R_H has been calculated from the relaxation time with the help of the Stokes−Einstein equation via the relation $R_H = (kTq^2/6\pi\eta)\tau$, where k is the Boltzmann constant, T absolute temperature, q the scattering vector, and η the viscosity.

Small-Angle X-ray Scattering. SAXS measurements were performed using a homemade camera with a KRATKY slit-collimation system, equipped with a linear 100 mm long wire PSD manufactured in the JINR Dubna.[44] With the sample−detector distance of 0.45 m and the X-ray wavelength $\lambda = 0.154$ nm, the q-range of 0.048−8.1 nm^{-1} was covered using one of two possible setups. The magnitude of the scattering vector is defined as $q = 4\pi \sin(\theta)/\lambda$, where 2θ is the scattering angle. Absolute intensity calibration was accomplished using a LUPOLEN standard sample. Scattering of methanol was subtracted as a background. The experimental temperature range was from −35 °C to 60 °C.

The form factor of the macromolecules studied was assumed to obey the Debye function[45] $I(q) = I(0)P(q)$ where $P(x) = 2(e^{-x} + x - 1)/x^2$ and $x = q^2R_G^2$. A least-squares fit of function $I(q)$ smeared by the length profile of the primary beam to the experimental SAXS intensities provided the values of the radius of gyration, R_G, and the scattering intensity extrapolated to zero angle, $I(0)$. The latter quantity was used to assess the molar mass of the macromolecules, employing the relation $M_w = I(0)N_A/c\Delta b^2$ where Δb and c are the excess scattering amplitude (in cm/g) and the concentration (in g/cm^3) of the polymer, respectively, N_A is the Avogadro number. Using $\Delta b = 3.2 \times 10^{10}$ cm/g (based on the partial volume of PHEMA in methanol, 0.785 cm^3/g), we obtained at 20 °C $M_w = 1.4 \times 10^5$ g/mol, a value close to the value determined by light scattering.

CHART 2

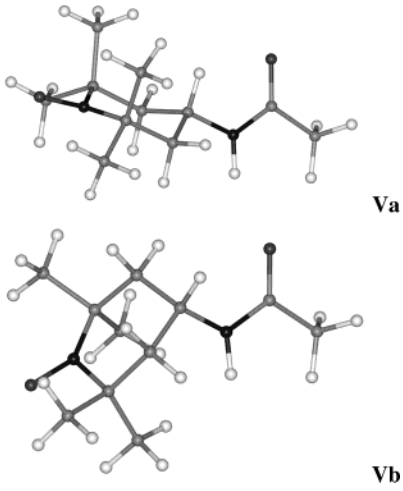

Va **Vb**

Quantum Chemical Modeling. The nitroxide moiety in the polymer system **IV** was truncated to 4-acetamido-2,2,6,6-tetramethylpiperidine-1-yloxyl **(V)** (Chart 2). Two conformers of this compound were considered, which represent structures with different puckering of the 2,2,6,6-tetramethylpiperidin-1-yloxyl ring. They were subjected to the full geometrical optimization at the UB3LYP/6-31+G* level of theory using the Gaussian98 suite of programs.[46] Thus, the unrestricted open-shell Hamiltonian was combined with the B3LYP (Becke's three-parameter exchange[47] and Lee, Yang, Parr correlation[48]) DFT (density functional theory[49]) functional and the standard split-valence basis set augmented with one set of polarization and diffuse functions.[50] Six-component *d*-type polarization functions were used. Located stationary points were verified to be minima by calculations of harmonic vibrational frequencies (all real for both conformers). The size of the system and its doublet character limit the level of theory at which **V** can be studied in a reasonable amount of time. For example, the UB3LYP/6-31+G* vibrational analysis of each conformer took ca. 12 days of CPU time on the R12000 processor of an SGI Origin 2000 supercomputer.

Results and Discussion

Rigid Limit Spectra. The components of ***A***- and ***g***-tensors of the nitroxide spin-label attached to PHEMA chains were determined in the usual way from rigid-limit ESR spectra of the spin-labeled copolymer measured in frozen methanolic solutions below 130 K. Best fits were achieved with Pearson VII line shape with $M \sim 1.5$ characterized by the parameters w^P_{prp} and w^P_{pll}. This corresponds to a combined Lorentzian−Gaussian line shape frequently observed in rigid-limit spectra. It should be noted that the line shapes of the well-resolved spectra are very sensitive to the A_{xx} and A_{zz} values but are less sensitive to the A_{yy} values. The uncertainty in A_{yy} was resolved

TABLE 1: *A*- and *g*-Tensor Components and Other Parameters Determined by Analysis of Rigid-Limit ESR Spectra of Spin-Labeled PHEMA Dissolved in Methanol

A_{xx}[G]pm	A_{yy}[G]	A_{zz}[G]	g_{xx}	g_{yy}	g_{zz}	w^{P}_{prp}[G]	w^{P}_{pll}[G]	M
7.12± 0.04	5.27± 0.17	36.22± 0.14	2.00858± 0.00001	2.00514± 0.00002	2.00140± 0.00003	2.37± 0.05	3.19± 0.14	1.50± 0.05

by adopting the values calculated from the isotropic nitrogen hyperfine splitting, which were determined from the motionally narrowed three-line spectra observed at higher temperatures. The best-fit values of ***A***- and ***g***-tensor components and several other parameters are given in Table 1. They were found to be practically independent of the PHEMA concentration. The best fits are characterized by correlation coefficients higher than 0.9986 at all the concentrations studied.

Slow Motional Spectra. When analyzing the slow-motional spectra, we started by using simple axially symmetric Brownian diffusion as model for spin-label dynamics. Later we tried various models of jump diffusion and completely anisotropic rotational diffusion characterized by three components of rotational tensor R_x, R_y, R_z, as well. The best fits of the experimental spectra, from both visual and statistical (e.g., correlation coefficients obtained from the NLSL program) points of view, were obtained when using the MOMD model with axially symmetric Brownian rotational diffusion (R_{prp} and R_{pll}) and with a local potential as model for the spin-label reorientation. The MOMD model, when applied to the system of nitroxide spin labels attached by short side chains (tethers) to the PHEMA main chain in solution, implies a preferred orientation for the axis of internal rotation of each attached nitroxide label with respect to the polymer main chain. However, due to the random distribution of polymer orientations, there is an isotropic distribution of these preferred orientations in the macroscopic sample. The nature of the preferred orientational distribution is determined by the shape of the ordering potential, which may be varied by means of potential parameters c^2_0, c^2_2, c^4_0, etc., and optimized during the fitting process. The three parameters mentioned above were found to be sufficient for the purpose of the present study. The tractable basis set characterized by the parameters[32] lemx = 14, lomx = 11, kmx = 8, mmx = 8, and ipnmx = 2 was found to be sufficient and was used for all calculations.

Examples of experimental ESR spectra of the spin-labeled PHEMA in methanol at given concentrations taken in an appropriate temperature range are presented in Figure 1 together with simulated, best fitting spectra. Fits of similar quality characterized by the correlation coefficients higher than 0.993 at all the concentrations studied and better than 0.997 at temperatures above 270 K were obtained (see Figure 2). The best-fit values of the fitting parameters shown in Figure 2 demonstrate general consistency of the model used. At all the concentrations investigated, the angle β first increases with increasing temperature, reaching maximum at approximately 250 K, and decreases when the temperature increases further. The isotropic inhomogeneous Lorentzian broadening w^L reaches minimum at temperatures close to 230 K and then increases with increasing temperature.

Ordering Potentials. The best-fit values of the three potential parameters employed characterize the shape of the ordering potential at a particular temperature and concentration. The

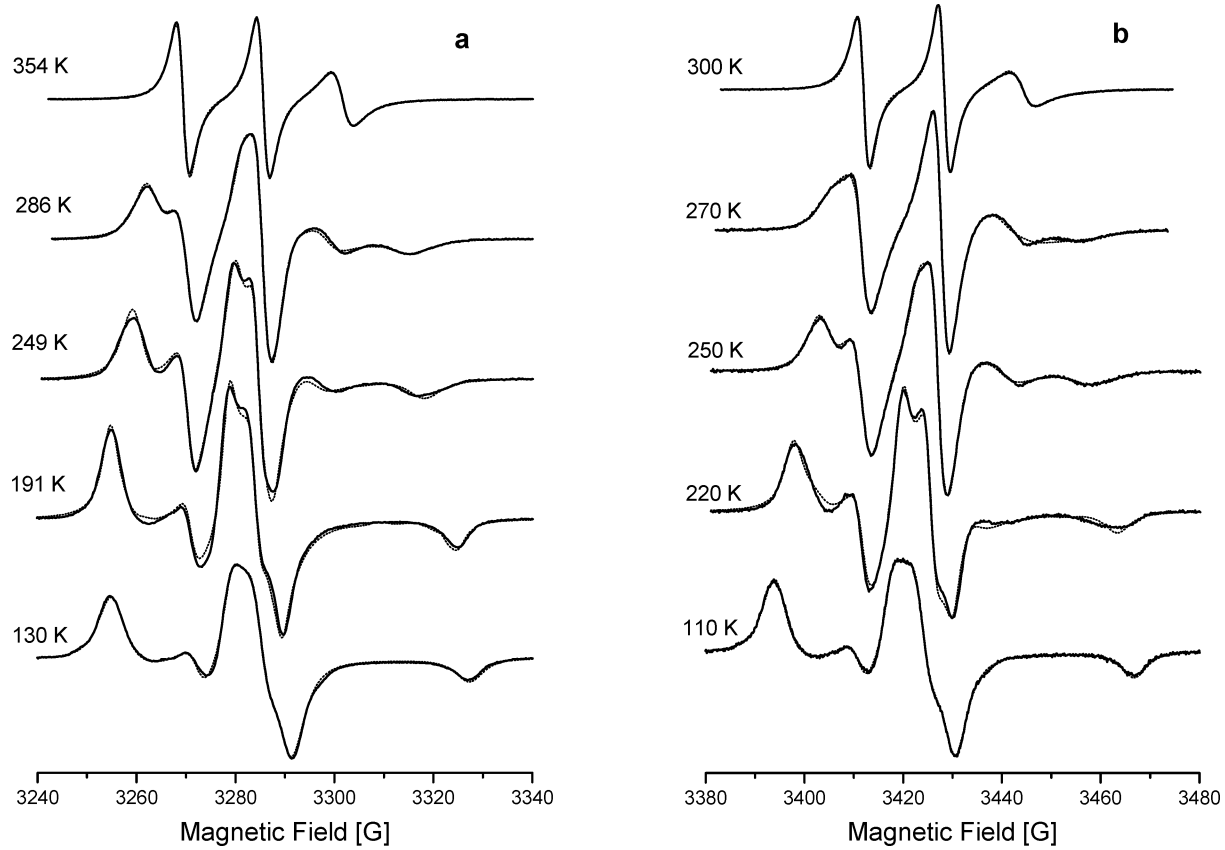

Figure 1. ESR spectra (experimental spectra−full lines; simulated spectra−dotted lines) of spin-labeled PHEMA in methanolic solution at given temperarures: (a) concentration of PHEMA 50 wt %; (b) concentration of PHEMA 2 wt %.

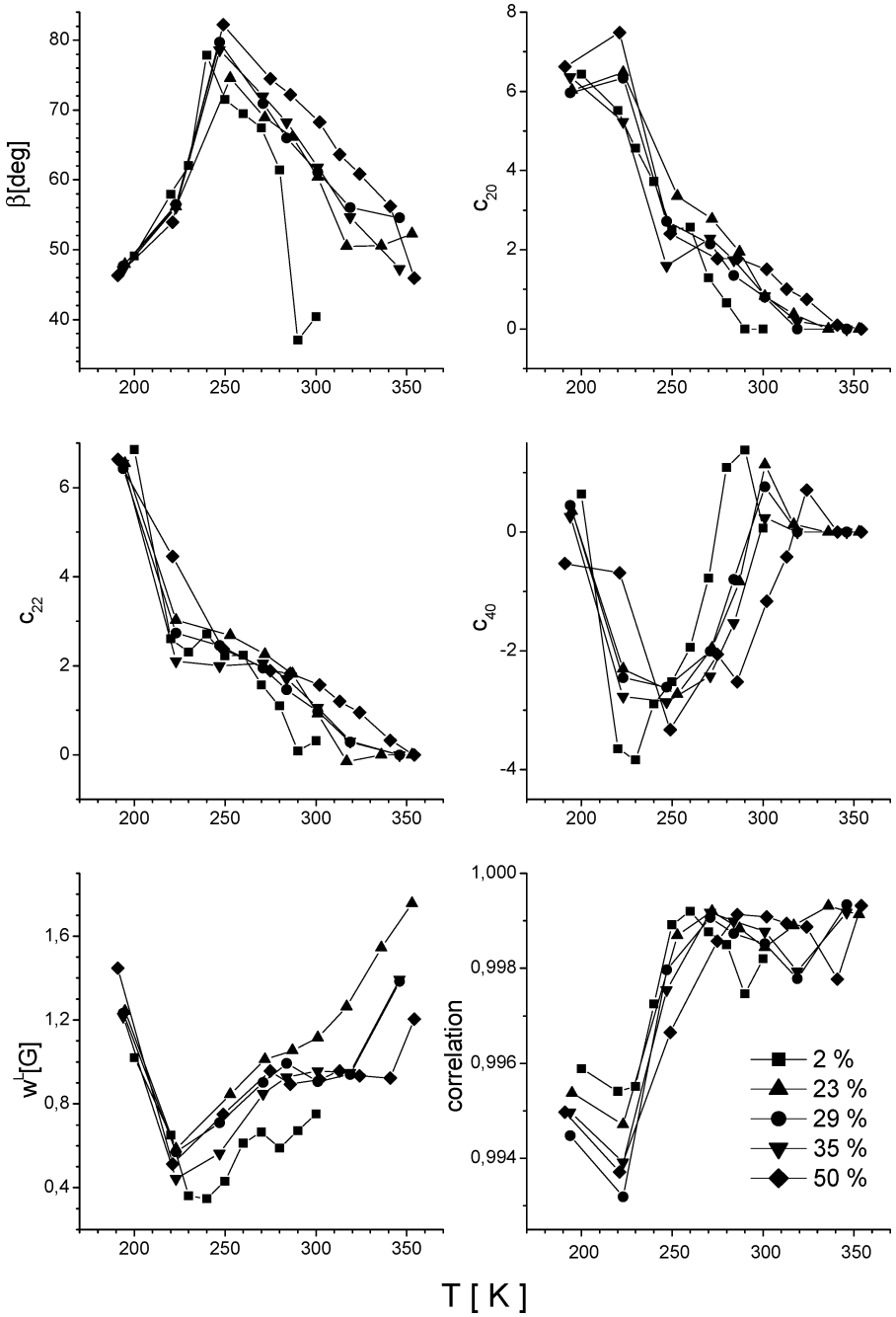

Figure 2. Temperature dependence of the best-fit values of the fitting parameters determined in analysis of ESR spectra of PHEMA in methanol for all the concentrations studied.

parameters c_0^2 and c_0^4 characterize the component of the ordering potential independent of the coordinate θ, and the parameter c_2^2 characterizes its rhombic distortion. Best-fit values of parameters c_0^2 and c_2^2 are positive and decrease with increasing temperature at all concentrations studied. Best-fit values of the parameter c_0^4 reach negative minimum values at temperatures close to 250 K and then increase toward zero with increasing temperature. Examples of typical shapes of the ordering potential $U(\theta,\varphi)$ in the coordinates θ and φ ($\theta = 0°$ for the directions in the symmetry plane of the piperidine moiety−in the *xz* plane of the nitroxide axis system defined in Chart 1 and $\varphi = 0°$ for the direction along the director) found in the 190−280 K temperature range are presented in Figure 3. The shapes show the probability distribution of effective orientation of the nitroxide rotational tensor symmetry axis with respect to the director. The appearance of two clearly visible maxima of the distribution separated by an angle of $2\varphi_{max}$ increasing from 60° to 100° ($\varphi_{max} \div 30-50°$) with temperature in this temperature range is typical of negative values of the parameter c_0^4 and positive c_0^2. The ordering potential keeps the plane of symmetry of the piperidine moiety (see Chart 1), and the maxima appear at $\theta = 0°$ and at $\theta = 180°$ as follows from the positive values of the parameter c_2^2.

Local PHEMA Dynamics. Rotational parameters R_S and R_I as determined by the fitting process of experimental spectra of spin-labeled PHEMA in methanol at all the concentrations studied are presented in Arrhenius-type plots in Figure 4. The plots differ at first sight by their nonlinearity for both rotational parameters from the published plots characterizing segmental dynamics of a number of polymers in dilute solution,[1−23,28,29] in particular from the recently published plots characterizing local dynamics of polystyrene in dilute solution, which are linear

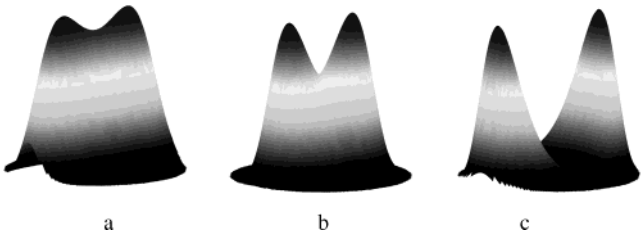

Figure 3. Population distribution of the instant orientation of the effective nitroxide rotational tensor symmetry axis with respect to the director as characterized by the parameters c_0^2, c_2^2, and c_0^4, determined by the fitting process applied to the ESR spectra of spin-labeled PHEMA in methanol at 50 wt % concentration, measured at (a) 191 K, (b) 221 K, and (c) 249 K. The potential decreases with increasing temperature as follows from the values of parameters c_K^L plotted in Figure 2.

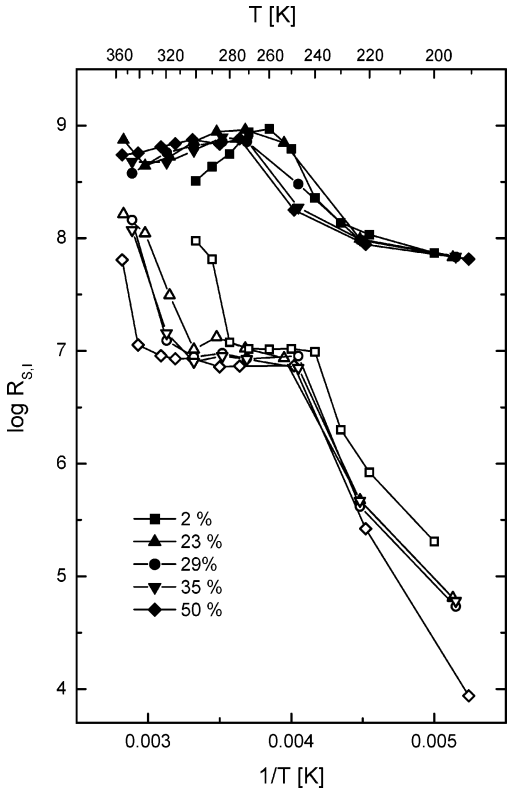

Figure 4. Arrhenius plots of rotational diffusion coefficients R_S (empty symbols) and R_I (full symbols) for the PHEMA in methanol for all concentrations studied.

for both rotational parameters regardless of the thermodynamic quality of the solvent.[33] The plots for the rotational parameter R_S exhibit a pronounced saddle part between the lower break temperature ~250 K and the upper break temperature, increasing from 290 K for the lowest concentration studied (2 wt %) up to 340 K for the 50 wt % concentration. In the temperature range between the lower and upper break temperatures, the polymer dynamics as characterized by parameter R_S, is more or less independent of temperature. These saddle parts are complemented by more or less linear regions for both lower and higher temperatures. The activation energy of the segmental rotational diffusion below the lower break temperature, $E_{exp} = 40 \pm 3$ kJ/mol, which is much higher than the activation energy of the viscous flow of methanol $E_\eta = 10.3$ kJ/mol, was determined from the plot. The rotational parameter R_I increases up to 260 K with increasing temperature and, surprisingly, slightly decreases when temperature increases above 260 K. The described features of the Arrhenius plot of rotational parameters

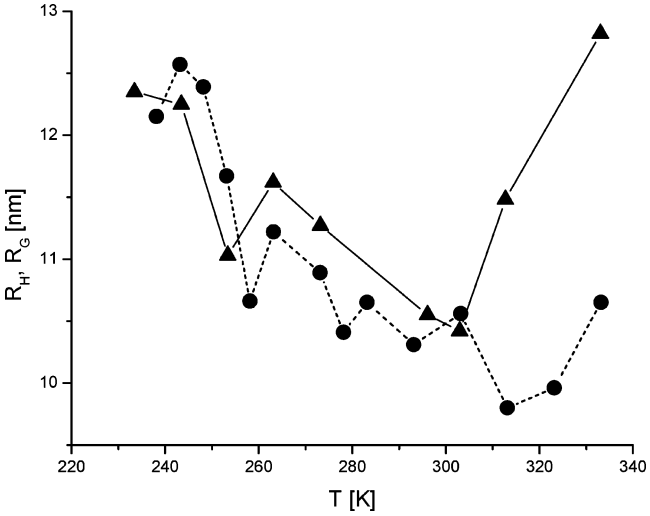

Figure 5. Hydrodynamic (RH ▲) and gyration (RG ●) radius of PHEMA coils in 2% methanolic solution determined by DLS and SAXS, respectively.

(Figure 4), and of the parameter characterizing local segmental mobility of the PHEMA chain, R_S, in particular, indicate a specific character of PHEMA local segmental dynamics in methanolic solution. The saddle part in the R_S plot has been found even for the lowest studied concentration of PHEMA in methanol (2 wt %), which corresponds to the concentration of polystyrene in the dilute solutions mentioned above. It follows that specific PHEMA − methanol interactions rather than high PHEMA concentration are operative here. The error in determination of both rotational parameters by the fitting process was estimated to be 10%.

In the previous study[27] we similarly obtained an atypical Arrhenius plot of rotational parameters characterizing local dynamics of poly(methyl methacrylate) (PMMA) in the ethyl acetate solvent. The appearance of break at approximately 300 K, dividing both R_S and R_I dependences into two parts characterized by different activation energies (higher for low-temperature parts), was explained by the conformational transition of the PMMA chain. Such conformational transition of the PMMA (and some other polymethacrylates) chain characterized by an increase of flexibility and a decrease in unperturbed dimensions of the polymer coil K_Θ by 8−25% above the transition temperature range was observed by Katime et al.[51] in the studies of molecular weight and temperature dependences of intrinsic viscosity of polymethacrylates in nonpolar organic solvents. For PMMA in ethyl acetate, the transition temperature range 318−328 K was found.

PHEMA belongs to the family of polymethacrylates and differs from the polymers studied by Katime et al.[51] in higher hydrophobicity (and subsequent insolubility in nonpolar solvents) due to the presence of the hydroxyethyl groups. Here we suggest the existence of conformational transition of PHEMA as an explanation for the observed temperature dependence of rotational parameters characterizing local dynamics of PHEMA in methanolic solutions, especially for the appearance of the saddle part clearly visible in Figure 4. This suggestion was supported by the results of dynamic light scattering (DLS) and X-ray scattering (SAXS) experiments presented in Figure 5 which show that both hydrodynamic (R_H) and gyration (R_G) radius of polymer globules in 2% methanolic solution of PHEMA in the temperature range 240−290 K decreases. The ratio R_G/R_H is known only in the Θ state and

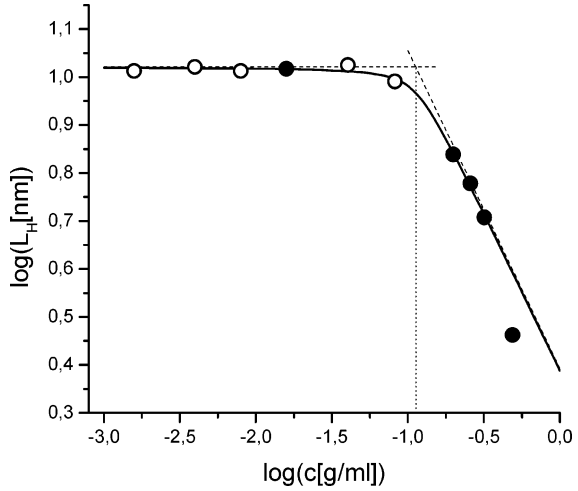

Figure 6. Concentration dependence of dynamic correlation length L_H of PHEMA in methanolic solution determined[40] by dynamic light scattering; dashed line indicates the crossover concentration at which the overlap of the polymer coils begins. Full symbols indicate data measured for the concentrations discussed in this paper.

for homogeneous spheres, where it attains the values 1.504 and 0.775, respectively.[52] This ratio is very sensitive to both the particle structure and polydispersity. Numerical equivalence of R_H and R_G determined by the two independent methods for spin-labeled PHEMA is probably a consequence of the fact that the polymer is polydisperse and probably branched.[52] DLS experiments revealed also the presence of large aggregates ($R_H \sim 200-300$ nm) in the solution. The amount of the PHEMA contained in the aggregates is negligible at temperature above 230 K but prevails below 220 K. This effect is probably responsible for the sharp decrease of R_S below the lower break temperature observed (Figure 4). Results of both DLS and SAXS experiments indicate increase of R_H and R_G above the upper break temperature observed for 2% solution (Figure 4).

In the paper dealing with the diffusion of paramagnetic tracers in nondilute methanolic solutions of PHEMA, we discussed[40] the concentration dependence of the dynamic correlation length, L_H, measured by dynamic light scattering (see Figure 6). At the specific concentrations above the overlap concentration $c^* \sim 10$ wt % of the polymer, practically the same values of L_H decreasing with increasing polymer concentration were obtained for methanolic solutions of both PHEMA and spin-labeled PHEMA. From Figure 6 it follows that the solutions containing 23−50 wt % of spin-labeled PHEMA studied in this paper can be characterized as entangled solutions. The measured dynamic correlation length, L_H, is equivalent to the hydrodynamic radius of the polymer chains at $c < c^*$ and is equivalent to the hydrodynamic blob size, ξ_H, for $c > c^*$. The observed increase in the upper break temperature (increase in the length of the saddle part in temperature units) with increasing concentration of the spin labeled PHEMA and simultaneously decreasing ξ_H (see Figure 6) indicates a dependence of local PHEMA dynamics on the strength of steric interactions in entangled solutions. The presence of a similar but shorter saddle part in the Arrhenius plot for the dilute solution (2 wt %), where neither entanglements nor intermolecular interactions are expected, suggests a strong influence of intramolecular steric interactions inside the highly flexible and compact PHEMA coil on its local dynamics in methanolic solution, similarly to the case of PMMA.

Correlation Between Quantum Chemical and MOMD Geometries. As mentioned earlier, MOMD calculation provides information on the form of the orienting potential $U(\theta,\varphi)$ which, through the Boltzmann exponential law, characterizes the population distribution of the instant orientation of the effective axis of internal rotation relative to the director. The orientation of the director, i.e., of a unit vector specified by $\varphi = 0°$, was considered to be identical with the orientation of the axis of internal rotation specified by single angle β, by which it is tilted in the *xz* plane relative to the *z* axis of the nitroxide axis system (Chart 1). We found that in the temperature range 190−280 K the orienting potential exhibits two maxima characterized by $\varphi_{max} = 30°-50°$, $\theta_1 = 0°$, $\theta_2 = 180°$, localized symmetrically with respect to the director and separated by the $2\varphi_{max}$ angle varying from 60° to 100°. Keeping in mind that the director tilt given by the β angle was found to vary between 50° and 80° in a given temperature range, MOMD simulations show that the most probable instantaneous orientations of the axis of nitroxide internal rotation, $\beta^S_{1,2} = \beta \pm \varphi_{max}$, calculated using β and φ_{max} angles determined for each of experimental spectra, increase with temperature increasing in the interval 190−280 K in the ranges $\beta^S_1 = 15°-30°$ and $\beta^S_2 = 85°-120°$.

The shapes of the ordering potential found in the low-temperature range for all the concentrations studied clearly indicate that the nitroxide moiety exists in two different conformations characterized by two different angles between the instantaneous orientation of the nitroxide internal rotation axis and the director. In addition, the exchange between the conformations should be slow enough on the time scale of the ESR experiment. The temperature dependence of all three potential parameters shows that the strength of ordering significantly decreases with increasing temperature. Specifically, the ordering becomes negligible at temperatures close to 300 K and higher.

To explain these results, we utilized the quantum chemical procedure described above. Thus, molecule **V** was subjected to a search for stable conformers, which resulted in the two UB3LYP/6-31+G* minima presented in Chart 2. They can be roughly described as structures containing different chair-like conformations of the piperidine ring. For the sake of simplicity, we consider the *x* axis of the nitroxide axis system to be oriented in the direction of the >N−O• bond. This is justified by the natural bond orbital analysis of the molecule **V** performed at the UB3LYP/6-31+G* level employing the NBO module of Gaussian98,[45] which revealed that the p_z orbital of the nitrogen atom is oriented nearly perpendicular to the >N−O• bond. Considering that the axis of nitroxide internal rotation is oriented in the direction of the NH−SL bond of the tether, it is easy to calculate the angle between the *x* axis of the nitroxide axis system and the symmetry axis of the rotational tensor of the nitroxide using coordinates of the atoms involved. By subtracting this angle from 90°, we obtain the diffusion angles $\beta^Q_1 = 11°$ and $\beta^Q_2 = 77°$ for each of the conformers, which are in reasonable agreement with the values $\beta^S_1 = 15°$ and $\beta^S_2 = 85°$ obtained by MOMD simulations at temperatures close to 190 K with the inclusion of the orienting potential. In particular, the value of the angle separating the two most probable orientations determined by MOMD simulation of the spectra measured for the lowest temperatures (close to 200 K), $2\varphi_{max} \sim 60°$, agrees very well with the value of this angle $\beta^Q_2 - \beta^Q_1 = 66°$ as determined by quantum chemical calculations performed for 0 K.

We also tried to verify the relative probabilities of occurrence of each conformation. MOMD simulation suggests that each conformation occurs with similar probability. This is due to the symmetry of the potential $U(\theta,\varphi)$ resulting in the equal probability for each of the extremes. The absolute energy of

the optimized conformers as provided by the quantum chemical calculations was converted to the relative probability of occurrence of each of the conformers using the Boltzmann exponential law. This calculation suggested that conformer **Va** is far more preferred than the more tightly packed conformer **Vb**. When putting relative energy for the conformer **Va** equal to zero, the relative energy of conformer **Vb** equals ca. 17 kJ/mol. We believe that this prediction is strongly affected by the reduced size of the model system subjected to quantum chemical computations: intra- and intermolecular interactions between polymer chain segments and the effects of interactions with solvent were not taken into account. These effects could increase the probability of occurrence of the more tightly packed conformer **Vb**. The appearance of two well-separated maxima of the orienting potential indicates that the conformational transitions between **Va** and **Vb** in the temperature range 190−280 K are slow with respect to the ESR time scale. At temperatures above the upper break temperature, the strength of steric interaction decreases and the probability of occurrence of the more tightly packed conformation **Vb** decreases. The orienting potential virtually diminishes and the nitroxide rotation can be characterized by a simple Brownian axially symmetric rotational diffusion characterized by the rotational parameters given in Figure 4 and by the angle β close to 40°.

Conclusions

A copolymer of HEMA with spin-labeled methacrylic acid units distributed randomly along the main chain at concentration ∼3 mol % was synthesized. ESR spectra of methanolic solutions of the copolymer at concentrations between 2 and 50 wt % were measured at X-band (9 GHz) over a broad temperature range. Temperature dependence of the R_S parameter characterizing the local segmental dynamics in PHEMA and of the other parameters characterizing local dynamics and conformation of the copolymer were determined by fitting experimental ESR spectra to the theoretical spectra calculated using the MOMD model. We found that Arrhenius plots of the rotational parameters exhibit an atypical nonlinear behavior characterized by two breaks at specific temperatures in the R_S plot. The difference between the lower break temperature (∼250 K for all the concentrations studied) and the upper break temperature was found to increase with increasing concentration of PHEMA in methanol. Local dynamics of the polymer was observed to be practically independent of temperature in the temperature range between both breaks. On the basis of our previous results and literature data, we concluded that, similarly to the behavior of PMMA and some other polymethacrylates in a number of nonpolar solvents, more hydrophobic PHEMA in methanol undergoes above the lower break temperature a conformational transition from a less compact to more compact conformation of the polymer chain. The decrease of polymer globule radius observed in 2% methanolic solution of PHEMA with the temperature increasing in the range close to the range at which the saddle part for this PHEMA concentration exists, determined by DLS and SAXS experiments, supports this conclusion. Intramolecular interactions in a dilute solution (2 wt %) in the range between both break temperatures, when PHEMA exists in a compact conformation, hinder local polymer dynamics. The contribution of the intermolecular interactions in entangled nondilute solutions (at polymer concentrations higher than ca. 20 wt %) is probably responsible for the same effect in more concentrated solutions and for the observed increase in the upper break temperature with increasing PHEMA concentration and simultaneously decreasing ξ_H. Analysis of the shape of the ordering potential, which constrains the preferred orientation of the effective axis of internal rotation of the tethered nitroxide, revealed the presence of two different conformations of the nitroxide moiety. The UB3LYP/6-31+G* quantum chemical calculations provided two conformational minima of the model system (nitroxide moiety plus tether) in a good agreement with the geometry required by the shape of the ordering potentials. However, the presence of the conformations revealed by these calculations may be accepted as an explanation of the obtained experimental data only providing that the effects omitted in the calculations, in particular the neglect of solvent effects and of interaction mediated by the polymer chain(s), would increase the probability of occurrence of the more tightly packed conformation.

Acknowledgment. This research was supported by the Grant Agency of the Academy of Sciences of the Czech Republic (project A4050306) and by the Academy of Sciences of the Czech Republic (project AVOZ4050913). We thank Č. Koňák and P. Kadlec for performing light scattering measurements and J. Pleštil (all IMC Prague) for participation in the SAXS experiments. Time allocation in the Czech Academic Supercomputer Centre and in the Mississippi Center for Supercomputer Research is gratefully acknowledged.

References and Notes

(1) Ediger, M. D. *Annu. Rev. Phys. Chem.* **1991**, *42*, 225.
(2) Waldow, D. A.; Ediger, M. D.; Yamaguchi, Y.; Matsushita, Y.; Noda, I. *Macromolecules* **1991**, *24*, 3147.
(3) Johnson, B. S.; Ediger, M. D.; Yamaguchi, Y.; Matsushita, Y.; Noda, I. *Polymer* **1992**, *33*, 3916.
(4) Adolf, D. B.; Ediger, M. D.; Kitano, T.; Ito, K. *Macromolecules* **1992**, *25*, 867.
(5) Johnson, B. S.; Ediger, M. D.; Kitano, T.; Ito, K. *Macromolecules* **1992**, *25*, 873.
(6) Yokotsuka, S.; Okada, Y.; Tojo, Y.; Sasaki, T.; Yamamoto, M. *Polym. J.* **1991**, *23*, 95.
(7) Ono, K.; Okada, Y.; Yokotsuka, S.; Sasaki, T.; Yamamoto, M. *Macromolecules* **1994**, *27*, 6482.
(8) Ono, K.; Ueda, K.; Yamamoto, M. *Polym. J.* **1994**, *26*, 1345.
(9) Ono, K.; Ueda, K.; Sasaki, T.; Murase, S.; Yamamoto, M. *Macromolecules* **1996**, *29*, 1584.
(10) Horinaka, J.; Amano, S.; Funada, H.; Ito, S.; Yamamoto, M. *Macromolecules* **1998**, *31*, 1197.
(11) Horinaka, J.; Aoki, H.; Ito, S.; Yamamoto, M. *Polym. J.* **1999**, *31*, 172.
(12) Horinaka, J.; Maruta, M.; Ito, S.; Yamamoto, M. *Macromolecules* **1999**, *32*, 1134.
(13) Horinaka, J.; Ito, S.; Yamamoto, M.; Tsujii, Y.; Matsuda, T. *Macromolecules* **1999**, *32*, 2274.
(14) Soutar, I.; Swanson, L.; Christensen, R. L.; Drake, R. C.; Phillips, D. *Macromolecules* **1996**, *29*, 4931.
(15) Heatley, F.; Begum, A. *Polymer* **1976**, *17*, 399.
(16) Heatley, F.; Wood, B. *Polymer* **1978**, *19*, 1405.
(17) Gronski, W.; Schäfer, T.; Peter, R. *Polym. Bull.* **1979**, *1*, 319.
(18) Glowinkowski, S.; Gisser, D. J.; Ediger, M. D. *Macromolecules* **1990**, *23*, 3520.
(19) Gisser, D. J.; Glowinkowski, S.; Ediger, M. D. *Macromolecules* **1991**, *24*, 4270.
(20) Gisser, D. J.; Ediger, M. D. *Macromolecules* **1992**, *25*, 1284.
(21) Spyros, A.; Dais, P.; Heatley, F. *Macromolecules* **1994**, *27*, 6207.
(22) Tylianakis, E. I.; Dais, P.; Heatley, F. *J. Polym. Sci., Part B: Polym. Phys.* **1997**, *35*, 317.
(23) Karali, A.; Dais, P.; Heatley, F. *Macromolecules* **2000**, *33*, 5524.
(24) Adolf, D. B.; Ediger, M. D. *Macromolecules* **1991**, *24*, 5834.
(25) Adolf, D. B.; Ediger, M. D. *Macromolecules* **1992**, *25*, 1074.
(26) Moe, N. M.; Ediger, M. D. *Macromolecules* **1995**, *28*, 2329.
(27) Pilař, J.; Labský, J. *J. Phys. Chem.* **1986**, *90*, 6038.
(28) Pilař, J.; Labský, J. *Macromolecules* **1991**, *24*, 4188.
(29) Pilař, J.; Labský, J. *Macromolecules* **1994**, *27*, 3977.
(30) Pilař, J.; Labský, J.; Marek, A.; Budil, D. E.; Earle, K. A.; Freed, J. H. *Macromolecules* **2000**, 33, 4438.
(31) Schneider, D. J.; Freed, J. H. In *Biological Magnetic Resonance*; Berliner, L. J., Reuben, J., Eds.; Plenum: New York, 1989; Vol. 8, p 1.

(32) Budil, D. E.; Lee, S.; Saxena, S.; Freed, J. H. *J. Magn. Reson.* **1996**, *Ser. A 120*, 155.
(33) Pilař, J.; Labský, J. *Macromolecules* **2003**, *36*, 913.
(34) Meirovitch, E.; Nayeem, A.; Freed, J. H. *J. Phys. Chem.* **1984**, *88*, 3454.
(35) *Encyclopedia of Polymer Science and Engineering*; Kroschwitz, J. I., Ed.; John Wiley & Sons: New York, 1985; Vol. 7, p 783; Vol. 9, p 486.
(36) Hamilton C.; Murphy, S. M.; Tighe, B. J. *Polymer* **1988**, *29*, 1887.
(37) Ratner, B. D.; Hoffman, A. *ACS Symp. Ser.* **1976**, *31*, 1.
(38) Pedley, D. G.; Skelley, P. J.; Tighe, B. J. *Br. Polym. J.* **1980**, *12*, 99.
(39) Wichterle, O.; Lím, D. *Nature* **1960**, *185*, 117.
(40) Marek, A.; Labský, J.; Koňák, Č.; Pilař, J.; Schlick, S. *Macromolecules* **2002**, 35, 5517.
(41) Kurosaki, T.; Takahashi, O.; Okawara, M. *J. Polym. Sci., Polym. Chem. Ed.* **1974**, *12*, 1407.
(42) Labský, J.; Pilař, J.; Lövy, J. *J. Magn. Reson.* **1980**, *37*, 515.
(43) Jakeš, J. *Collect. Czech. Chem. Commun.* **1995**, *60*, 1781.
(44) Chernenko, S.; Cheremukhina, G.; Fateev, O.; Smykov, L.; Vasilev, S.; Zanevsky, Yu.; Kheiker, D.; Popov, A. *Nucl. Instrum. Methods* **1994**, *A348*, 261.
(45) Debye, P. J. *J. Phys. Colloid Chem.* **1947**, *51*, 18.
(46) Frisch, M. J.; Trucks, G. W.; Schlegel, H. B.; Scuseria, G. E.; Robb, M. A.; Cheeseman, J. R.; Zakrzewski, V. G.; Montgomery, J. A., Jr.; Stratmann, R. E.; Burant, J. C.; Dapprich, S.; Millam, J. M.; Daniels, A. D.; Kudin, K. N.; Strain, M. C.; Farkas, O.; Tomasi, J.; Barone, V.; Cossi, M.; Cammi, R.; Mennucci, B.; Pomelli, C.; Adamo, C.; Clifford, S.; Ochterski, J.; Petersson, G. A.; Ayala, P. Y.; Cui, Q.; Morokuma, K.; Malick, D. K.; Rabuck, A. D.; Raghavachari, K.; Foresman, J. B.; Cioslowski, J.; Ortiz, J. V.; Stefanov, B. B.; Liu, G.; Liashenko, A.; Piskorz, P.; Komaromi, I.; Gomperts, R.; Martin, R. L.; Fox, D. J.; Keith, T.; Al-Laham, M. A.; Peng, C. Y.; Nanayakkara, A.; Gonzales, C.; Challacombe, M.; Gill, P. M. W.; Johnson, B. G.; Chen, W.; Wong, M. W.; Andres, J. L.; Head-Gordon, M.; Replogle, E. S.; Pople, J. A. *Gaussian 98*, revision A.11.4; Gaussian, Inc.: Pittsburgh, PA, 2002.
(47) Becke, A. D. *J. Chem. Phys.* **1993**, *98*, 5648.
(48) Lee, C. T.; Yang, W. T.; Parr, R. G. *Phys. Rev. B* **1988**, *37*, 785.
(49) Parr, R. G.; Yang, W. T. *Density-Functional Theory of Atoms and Molecules*; Oxford University Press: Oxford, 1989.
(50) Szabo, A.; Ostlund N. S. *Modern Quantum Chemistry*; McGraw-Hill: New York, 1982.
(51) Katime, I. A.; Garay, M. T., Francois, J. *J. Chem. Soc., Faraday Trans. 2* **1985**, *81*, 705 and references therein.
(52) Štěpánek, P.; Koňák, Č. *Advances in Colloid and Interface Science* **1984**, *21*, 195.